ACI STRUCTURAL JOURNAL TECHNICAL PAPER

Title No. S119-S23

# Modeling of Ultra-High-Performance Fiber-Reinforced Concrete in Shear

by Zhongyue Zhang, Frank J. Vecchio, Evan C. Bentz, and Stephen J. Foster

*Ultra-high-performance fiber-reinforced concrete (UHPFRC) is a material attracting increased use to solve practical engineering problems. Although significant research has been undertaken to develop constitutive models for finite element modeling of steel fiber-reinforced concrete (SFRC), the reliability of these models in characterizing UHPFRC remains unassessed. Specifically, only limited research is available on rational models for describing post-cracking tension and shear-related mechanisms in UHPFRC under various loading conditions. To address these modeling deficiencies, this study investigates existing SFRC material models for their suitability in finite element analysis of UHPFRC. Localized behavior at cracks is investigated, leading to improvements in crack-related formulations through the inclusion of effective aggregate size. An embedded steel reinforcement rupture formulation for elements subjected to tension is also implemented to better capture rupture strains in specimens containing conventional reinforcement. Validation studies are provided to demonstrate the effectiveness of the proposed model improvements.*

**Keywords:** finite element modeling; reinforcement rupture; shear; steel fiber-reinforced concrete (SFRC); ultra-high-performance fiber-reinforced concrete (UHPFRC).

## INTRODUCTION

Developed in the 1990s,[1] ultra-high-performance fiber-reinforced concrete (UHPFRC) is a cementitious composite with superior mechanical properties. With compressive strengths of more than 200 MPa (29 ksi) achievable and advanced durability characteristics,[2,3] this material lends itself to innovative and efficient solutions to many practical design problems. For example, its low permeability characteristic results in the ability to resist aggressive environments, an essential property for the rehabilitation of deteriorating structures and providing significant environmental benefits.[4] Although the great potential of UHPFRC for structural applications has been successfully demonstrated, widespread use remains limited. Several obstacles remain, including an incomplete understanding of its mechanical properties and the absence of proven analysis methods and unified design procedures. In particular, there has been limited advancement in the development of rational constitutive models and a lack of easily employed finite element models for calculating the flexural and shear behavior of UHPFRC structural components.

Much research has been undertaken in the development of numerical models for steel fiber-reinforced concrete (SFRC); nevertheless, large levels of uncertainty persist in current finite element analysis methods, producing excessively large scatter in results. For example, in 2020, the CEB-FIP *fib* Working Group WG 2.4.2, Modeling of Fiber Reinforced Concrete Structures, held a blind modeling competition to predict the behavior of an SFRC T-beam tested under shear.[5] Highly detailed descriptions of the material properties, structural details, and loading criteria were provided to all participants. The resulting 37 entries submitted by participants showed significant variability in the performance of typical numerical models used for simulating the behavior of fiber-reinforced concrete. In the related study by Barros et al.,[5] the uncertainties within these models are made apparent by the large spreads seen in both the load-deflection and strain-deflection responses shown in Fig. 1. The ratio of the predicted to actual failure load ranged from 0.28 to 2.37, with the predicted deflection at failure showing even greater scatter. The corresponding predicted strain at failure demonstrated a variability upwards of 600%. These dramatically varying results indicate the need for a deeper understanding of the modeling tools, constitutive relationships, and assumptions used for modeling fiber-reinforced concrete.

To address the uncertainty in modeling methods and the general lack of analytical work on UHPFRC in shear, this study investigates the appropriateness of existing finite element-based constitutive models developed principally for conventional SFRC—specifically, in their ability to provide reliable simulations of the response of UHPFRC structures. For this study, VecTor2, a nonlinear finite element analysis program developed at the University of Toronto to analyze two-dimensional membrane structures was used.[6] For reinforced concrete elements subjected to in-plane stresses, VecTor2 calculates the response using a smeared, rotating crack formulation based on the Modified Compression Field Theory (MCFT)[7] and the Disturbed Stress Field Model (DSFM).[8] The program uses a total load iterative procedure based on a secant stiffness formulation, giving a numerically robust and stable performance with good convergence characteristics.

Data from five large-scale UHPFRC pure shear tests previously conducted at the University of Toronto[9] were used to examine the suitability of current models for determining the load-deformation response, ultimate strength, and failure mode of UHPFRC shear-critical elements. Localized

*ACI Structural Journal*, V. 119, No. 1, January 2022.
MS No. S-2021-088.R1, doi: 10.14359/51733012, received June 6, 2021, and reviewed under Institute publication policies. 

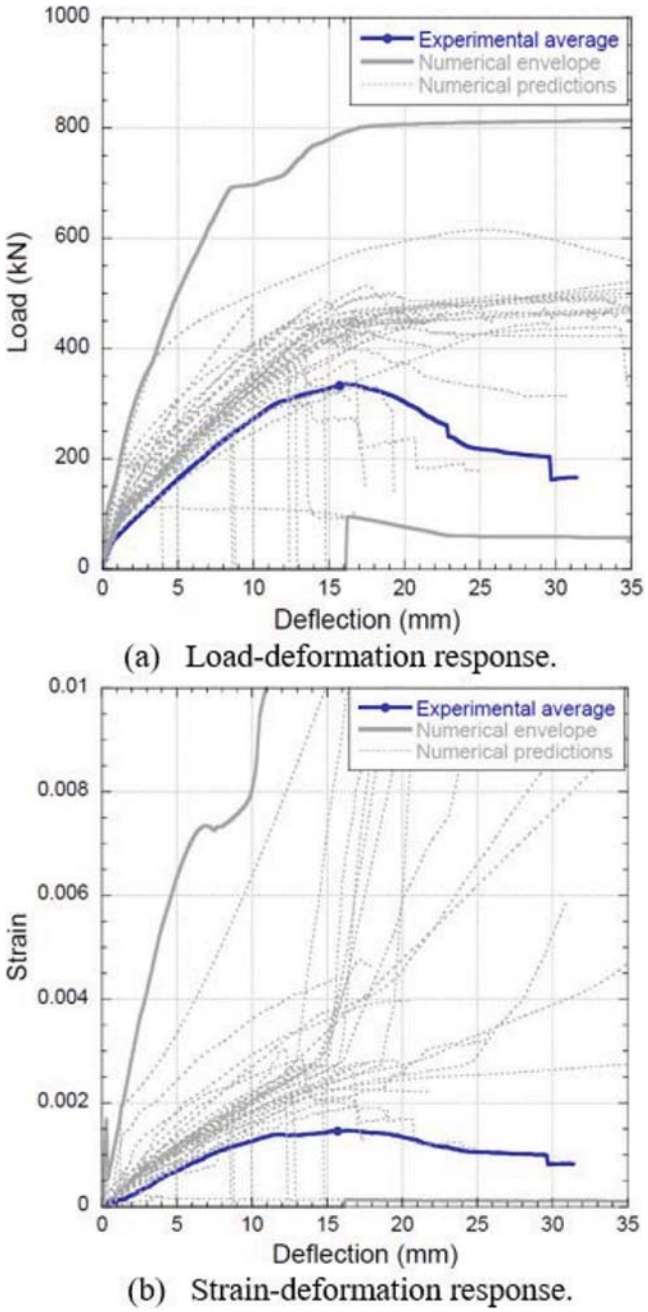


*Fig. 1—Comparison between experimental results and finite element predictions.*[5]

behavior at cracks was specifically considered, resulting in improvements to current crack width formulations. In addition, a steel reinforcement rupture model was formulated to capture the potential for reinforcement rupture in highly ductile members, a characteristic of UHPFRC structures. Finally, validation studies were conducted to verify the models using experimental results found in the literature.

## RESEARCH SIGNIFICANCE

A significant obstacle to applying UHPFRC is the limited work undertaken to date, both experimentally and numerically, to investigate its post-cracking tension and shear-related behavior under various loading conditions. This study addresses this insufficiency by identifying weaknesses in current finite element models developed principally for SFRC when analyzing UHPFRC. These investigations will facilitate the development of improved models for more accurate numerical simulations. A robust finite element model is crucial to the safe design of UHPFRC by providing valuable insight into UHPFRC behavior when full-scale experimental tests are too costly and time-consuming.

## OVERVIEW OF STATE OF ART

### Ultra-high-performance fiber-reinforced concrete

In the 1990s, ultra-high-performance concrete, originally known as reactive powder concrete, was first developed as a result of the quest to further improve the mechanical properties of concrete. This highly homogeneous cementitious composite is characterized by high portland cement content, small aggregate sizes, silica fume, and low water-cement ratios ($w/c$). These constituents produce a dense, smooth matrix, resulting in a material with enhanced performance, durability, strength, and toughness compared with normal- and high-strength concrete. It was well established that the use of small, discrete fibers as reinforcement significantly improves the ductility and tensile strength of concrete. Thus, ultra-high-performance concrete generally contains a high dosage of steel fibers to achieve ductile behavior.

### Experimental investigations

It has been shown that the mechanical properties of UHPFRC are influenced by a wide range of parameters such as curing conditions, packing density, and the characteristics of the added steel fibers. For example, in investigating the effect of steel fiber properties and reinforcement ratio on flexural response, Yoo and Yoon[10] found that deformed fibers, such as hooked-end and twisted steel fibers, generally increase the tensile strength, strain strength, and the strength of UHPFRC members.

To date, research programs have investigated UHPFRC under a variety of loading conditions including static, impact, and blast. Yang et al.[11] first studied the effect of longitudinal reinforcement ratio on flexural behavior and found that UHPFRC can redistribute stresses through multiple cracks forming before fiber pullout. The effect of reinforcement ratio on UHPFRC flexural behavior was also studied by Yoo et al.,[12] who found that the reinforcement ratio significantly affected its cracking behavior. In investigating the efficacy of numerical models developed for reinforced concrete beams in analyzing UHPFRC, Singh et al.[13] tested four full-scale beams with varied spans and cross sections. Finally, Kodur et al.[14] analyzed the failure characteristics of UHPFRC beams containing large aggregates under flexural and shear loading.

Most recently, Yap[9] tested five large-scale UHPFRC panel elements under monotonic pure shear to investigate the effect of reinforcement conditions on shear strength. All five panels had a nominal dimension of 1625 x 1625 mm (64 x 64 in.) and a thickness of 200 mm (7.9 in.). All panels contained 1.0% in volume of hooked-end steel fibers and 1.0% straight fibers. Three panels contained conventional reinforcement in only one direction to investigate the effect of the shear demand at the crack on shear strength. One panel also contained no conventional reinforcement to investigate

the shear capacity of the matrix. The panels were loaded using the shell element tester at the University of Toronto; refer to Appendix A.* Additional information on the details and results of these tests can be found elsewhere.[9]

### Finite element investigations

Limited research is available in the literature on finite element (FE) modeling of UHPFRC. Foster et al.[15] and Voo et al.[16] report achieving good results using the variable engagement model when modeling UHPFRC beams failing in shear. Foster et al.[15] used a nonlocal approach to eliminate mesh size effects, demonstrating a good correlation for the test specimen SB7 reported in Voo et al.[17] Chen and Graybeal[18] investigated the applicability of using the concrete damage plasticity (CDP) model available in FE software to simulate the load-deflection responses of UHPFRC girders subjected to shear and flexure. Singh et al.[13] validated the applicability of the CDP model for simulating the behavior of large-scale UHPFRC beams. Franssen et al.[19] investigated a new modeling approach in VecTor2 for UHPFRC-strengthened concrete members. Although some of these FE investigations produced promising results, many of them considered limited test data and relied upon extensive material testing to calibrate the models.

## CONSTITUTIVE MODELING

### Variable Engagement Model

The Variable Engagement Model (VEM), developed by Voo and Foster,[20] describes the peak and post-peak behavior of SFRC composites subjected to uniaxial tension. This model's primary assumption is that the tensile behavior can be expressed as a sum of the concrete and fiber contributions. The effect of individual, randomly orientated, and discontinuous fibers can then be summed over three-dimensional (3-D) space to describe the overall behavior of the composite.

In the VEM, the tensile stress attained by the fibers is evaluated as

$$f_f = K_f K_d \frac{l_f}{d_f} V_f \tau_b \tag{1}$$

where $K_f$ is the global orientation factor; and $K_d$ is a damage factor that accounts for the loss in bond efficiency due to the pullout of adjacent fibers. In general, $K_d$ can be taken as 1.0 for concrete containing a conventional volume of fibers. The variables $d_f$, $l_f$, and $V_f$ are the fiber diameter, length, and volume fraction, respectively, and $\tau_b$ is the interfacial shear stress between the fibers and the matrix. In lieu of shear stress data, Voo and Foster[20] suggested using the following equation for $\tau_b$

$$\tau_b = \begin{pmatrix} 2.5 f_t' \text{ for concrete with hooked-end fibers} \\ 2.0 f_t' \text{ for concrete with straight fibers} \\ 1.2 f_t' \text{ for mortar with hooked-end fibers} \\ 1.0 f_t' \text{ for mortar with straight fibers} \end{pmatrix} \tag{2}$$

*The Appendix is available at **www.concrete.org/publications** in PDF format, appended to the online version of the published paper. It is also available in hard copy from ACI headquarters for a fee equal to the cost of reproduction plus handling at the time of the request.

The global orientation factor, $K_f$, accounts for fiber orientation and engagement. Where fracture of the fibers is possible, $K_f$ is determined by numerical integration

$$K_f = \frac{4}{\pi l_f^2} \int_0^{\theta crit} \left[ \max\left( l_{a,crit} - w_{cr}, 0 \right) \right]^2 d\theta \tag{3}$$

$$l_{a,crit} = \min(l_c / 2 + w_e, l_f / 2) \tag{4}$$

$$l_c = \frac{d_f}{2} \frac{f_t'}{\tau_b} \tag{5}$$

$$\theta_{crit} = \tan^{-1}\left( w_{cr} / \left( \alpha_1 l_f \right) \right) \tag{6}$$

where $l_{a,crit}$ is the critical embedment length for fiber fracture; $w_{cr}$ is the average crack width; $l_c$ is the critical length of the fiber; $f_t'$ is the tensile strength of the concrete; $\theta_{crit}$ is the critical angle of orientation from the normal direction to the crack surface; and $\alpha_1$ is an engagement constant taken as $\alpha_1 = 1/(3.5 l_f/d_f)$.[16]

Where fiber fracture is not possible, the critical embedment length for fracture is assumed to equal to $l_f/2$ and the orientation factor equation reduces to the following

$$K_f = \frac{\tan^{-1}(w_{cr} / \alpha)}{\pi} \left( 1 - \frac{2 w_{cr}}{l_f} \right)^2 \tag{7}$$

## DIVERSE EMBEDMENT MODEL AND SIMPLIFIED DIVERSE EMBEDMENT MODEL

The Diverse Embedment Model (DEM),[21] and later the Simplified Diverse Embedment Model (SDEM),[22] were proposed for capturing the tensile behavior of SFRC members with both straight and hooked-end steel fibers. Similar to the VEM, these models consider the randomness in fiber inclination angle and fiber embedment lengths. In contrast to the VEM, these models also consider the effect of unsymmetrical anchorage of hooked-end steel fibers on the constitutive relationship. Both the DEM and SDEM separately evaluate the tensile stress due to frictional bond behavior and the mechanical anchorage effects from the pullout of a single straight or hooked-end fiber.

In the SDEM, the tensile stress attained by the steel fibers, $f_f$, for the two different types of steel fibers is taken as

$$f_f = \begin{cases} f_{st} & \text{for straight fibers} \\ f_{st} + f_{eh} & \text{for hooked-end fibers} \end{cases} \tag{8}$$

For both hooked-end and straight fibers, the fiber tensile stress attained by the frictional bond between the embedded fibers and the concrete, $f_{st}$, is calculated as

$$f_{st} = \alpha_f V_f K_{st} \tau_{f,max} \frac{l_f}{d_f} \left( 1 - \frac{2 w_{cr}}{l_f} \right)^2 \tag{9}$$

$$K_{st} = \begin{cases} \frac{\beta_f}{3} \frac{w_{cr}}{s_f} & \text{for } w_{cr} \le s_f \\ 1 - \sqrt{\frac{s_f}{w_{cr}}} + \frac{\beta_f}{3} \sqrt{\frac{s_f}{w_{cr}}} & \text{for } w_{cr} > s_f \end{cases} \tag{10}$$

$$\tau_{f,max} = 0.396\sqrt{f_c'} \tag{11}$$

where $\alpha_f = 0.5$ for a 3-D infinite element; $s_f$ is the slip corresponding to the full bond strength taken as 0.01; $\beta_f = 0.6$; and $w_{cr}$ is the average crack width. $\tau_{f,max}$ and $f_c'$ are in MPa.

For hooked-end fibers, additional stress is attained through the mechanical anchorage of the hooked ends. This additional stress, $f_{eh}$, is calculated as

$$f_{eh} = \alpha_f V_f K_{eh} \tau_{eh,max} \frac{2\left(l_f - 2w_{cr}\right)}{d_f} \tag{12}$$

$$K_{eh} = \begin{cases} \beta_{eh}\left[\frac{2}{3}\frac{w_{cr}}{s_f} - \frac{1}{5}\left(\frac{w_{cr}}{s_f}\right)^2\right] & \text{for } w_{cr} \le s_{eh} \\ 1 + \left(\frac{7\beta_{eh}}{15} - 1\right)\sqrt{\frac{s_{eh}}{w_{cr}}} - \frac{2\left(\sqrt{w_{cr}} - \sqrt{s_{eh}}\right)^2}{l_f - l_i} & \text{for } s_{eh} < w_{cr} \le \frac{l_f - l_i}{2} \\ \left(\frac{l_i - 2w_{cr}}{2l_i - l_f}\right)^2 K_{eh,i} & \text{for } \frac{l_f - l_i}{2} \le w_{cr} < \frac{l_i}{2} \end{cases} \tag{13}$$

$$\tau_{eh,max} = 0.429\sqrt{f_c'} \tag{14}$$

where $l_i$ is the distance between mechanical anchorages for hooked-end fibers, $K_{eh,i}$ is $K_{eh}$ at $w_{cr} = (l_f - l_i)/2$; $\beta_{eh} = 0.8$; and $s_{eh} = 0.1$.

A variation of the SDEM was developed and implemented by Franssen et al.[19]; refer to Appendix B for details.

The VEM, the SDEM, and the Franssen models differ substantially in fiber bond stresses used in their formulations; Appendix C provides a comparison. In Table C.1, note, in particular, the large discrepancies in bond stress for straight fiber in concrete. Compared with the other two models, the SDEM assumes a much lower fiber bond stress.

## Parametric study

A parametric study was undertaken to investigate the influence of key parameters on the behavior of UHPFRC as obtained from nonlinear FE analysis. The specimen modeled in this study was Panel YS1, one from the series of UHPFRC panels tested in pure shear by Yap.[9] The parameters investigated included concrete tensile strength, maximum aggregate size, crack spacing, element size and thickness, and randomness in material strengths.

Panel YS1 was a 1625 x 1625 mm (64 x 64 in.) and 200 mm (7.9 in.) thick element subjected to monotonically increasing pure membrane shear loading. The panel's reinforcement consisted of conventional in-plane orthogonal reinforcement (0.86%) in each direction, hooked-end fibers (1.0%), and short straight fibers (1.0%). The concrete compressive strength was 171 MPa (24.8 ksi). Refer to Yap[9] for additional details and properties. For simplicity, Panel YS1 was modeled as a single four-noded plane stress rectangular element. Both the fiber reinforcement and conventional reinforcement were modeled as smeared, and the SDEM was used for the post-cracking tension constitutive model for UHPFRC. Analyses were done under force-controlled loading.

The inclusion of steel fibers in concrete is known to improve resistance to cracking when compared to conventional reinforced concrete. Current research has shown that the cracking strength of a UHPFRC member is dependent on many factors, such as fiber type, shape, and volume content.[12] As such, a UHPFRC element such as Panel YS1 is expected to have a larger experimental cracking strength than the default cracking stress of $0.33\sqrt{f_c'}$ (MPa) ($4.0\sqrt{f_c'}$ [psi]) used. In addition to the default value, three other tensile strengths were investigated, ranging up to $0.6\sqrt{f_c'}$ (MPa) ($7.3\sqrt{f_c'}$ [psi]). The analysis results showed that as the concrete tensile strength increases, the applied shear stress at first cracking increases proportionally, but the post-cracking response remains unaffected; refer to Fig. D.1 in Appendix D. Thus, concrete tensile strength has little influence on the element's calculated ultimate shear strength or post-cracking deformation response.

It is commonly assumed that stress is transferred across a crack through aggregate interlock mechanisms, significantly influencing the post-cracking behavior of concrete subjected to shear-critical conditions. The maximum shear stress that can be transmitted across the crack is dependent, in part, on the concrete aggregate size. Analyses were conducted for aggregate sizes ranging from 1 to 20 mm (0.04 to 0.80 in.). The influence on the computed responses was significant with, as expected, larger aggregate sizes resulting in stiffer and stronger responses; refer to Fig. D.2. Because UHPFRC composition generally does not contain coarse aggregate, it would be appropriate to assume smaller aggregate sizes in the FE modeling, typically less than 2 mm (0.08 in.). However, despite UHPFRC's lack of coarse aggregate, the crack surface is considerably rough due to the presence and action of steel fibers. Thus, the use of a larger "effective aggregate size" may be warranted.

The addition of fibers in SFRC allows for the formation of more closely spaced cracks, thereby affecting tension-stiffening and aggregate interlock behaviors. Software allows for either user input crack spacings or program-calculated values according to the crack spacing formulation developed by Deluce et al.[23] for SFRC. From the analyses conducted (refer to Fig. D.3), it is evident that reduced crack spacings (and thus reduced crack widths) have significant and counteracting consequences. Initially, decreasing the crack spacing results in a stiffer and stronger element shear response due to improved aggregate interlock. After a certain point, however, the reduced crack widths result in less engagement of the fibers, and the shear response degrades. Note that in the actual test of YS1, the observed crack spacing was approximately 50 mm (2.0 in.), whereas the Deluce model gives a calculated spacing of 20 mm (0.8 in.). Hence, this model, developed for tension-softening SFRC, appears not directly applicable to UHPFRC.

In VecTor2, mesh size effects, as they relate to slip on cracks, are eliminated by modifying the slip calculations to assume the same maximum crack width regardless of the element size. To confirm this, Panel YS1 was reanalyzed using a 10 x 10 element grid. The results were unchanged relative to the one-element model (refer to Fig. D.4). In addition, the effect of element thickness on the one-element model was also investigated, and the results are shown in Fig. D.5. Decreasing the element thickness appears to slightly improve the post-cracking capacity and the shear deformation capacity of the element. This is because, in the SDEM, the fiber efficiency factor is affected by the element thickness. As the element thickness decreases, fibers are more likely to be orientated parallel to the loading direction, increasing fiber bridging action's effectiveness and improving the ultimate strength capacity.

Finally, parametric stochastic analyses were performed to account for uncertainties in material properties and investigate the influence of the variability of properties within the specimen. Stochastic simulations using both the Monte Carlo sampling and Monte Carlo sampling with random field spatial variation options available in VecTor2[24] were performed to consider uncertainties in the concrete and steel material properties. The primary variables were the concrete compressive strength (also affecting the concrete tensile strength and elastic modulus) and the reinforcement and fiber strengths. The Bartlett and MacGregor model was used for concrete strength variation, and the Nowak and Szerszen model was used for reinforcement yield strength distribution. Shown in Fig. D.6 is the result of the Monte Carlo sampling with random field spatial variation. The analyses suggest that the behavior of a shear-critical UHPFRC element is highly sensitive to material variability, including significant influences on the calculated strength, deformation capacity, and failure mode.

## ENHANCEMENTS TO CONSTITUTIVE MODELING

### Reinforcement rupture

In UHPFRC containing conventional steel reinforcement, the embedded reinforcement can rupture at lower average strain values than would a bare bar due to the concrete cracking behavior and high bond strength. UHPFRC pure shear panels YS1 and YS5,[9] exhibited a highly ductile response ending in reinforcement rupture. As such, to accurately predict the deformation capacity of UHPFRC members through nonlinear FE analysis, it is necessary to account for the possibility of reinforcement rupture. One effective formulation is the tension-stiffening model by Lee et al.,[25] developed based on a series of analytical parametric studies investigating factors that influence average concrete tensile stresses after reinforcement yielding. In this model, the post-yielding reinforcement stresses at crack locations are calculated from force equilibrium and are used to determine the average strain conditions resulting in reinforcement rupture.

Although the Lee model can reasonably predict reinforcement rupture in most situations, it requires additional calculations that are typically not performed when using other tension-stiffening models. Thus, using the Lee model as the basis, a simplified model for reinforcement rupture using regression analysis was developed. It can be combined with the Bentz[26] formulation (the default model in VecTor2) and other simple tension-stiffening models.

Mayer and Eligehausen,[27] Moreno et al.,[28] Kang et al.,[29] and Nguyen et al.[30] tested a total of seven normal-strength reinforced concrete members under direct uniaxial tension until rupture of the reinforcement was achieved. The regression analysis used these experimental specimens to obtain a simplified numerical model for reinforcement rupture.

Multiple variables and combinations of variables were investigated to identify which material properties affect the reinforcement rupture strain. These included concrete compressive strength, $f_c'$ (MPa); reinforcement yield strength, $f_y$ (MPa); reinforcement ratio, $\rho_s$; reinforcement diameter, $d_b$ (mm); reinforcement ultimate strength, $f_u$ (MPa); and concrete tensile strength, $f_t'$ (MPa). The dependent variable to be predicted was the ratio between the embedded reinforcement rupture strain and the bare bar rupture strain, $\varepsilon_{rupt,embed}/\varepsilon_{rupt,bar}$. The regression analysis determined that using a combination of individual variables as the independent variable worked best with $d_b(f_u - f_y)/f_t'$ producing the tightest fit. Based on this, the following simplified equation for predicting the reinforcement strain at rupture was derived

$$\frac{\varepsilon_{rupt,embed}}{\varepsilon_{rupt,bar}} = \gamma = \frac{7}{25} + 213 \cdot 10^{-6} \cdot d_b \frac{f_u - f_y}{f_t'} \tag{15}$$

$$\frac{1}{3} \le \gamma \le 1.0 \tag{16}$$

$$\varepsilon_{rupt,embed} = \varepsilon_{rupt,bar} \cdot \gamma \tag{17}$$

where $\varepsilon_{rupt,embed}$ is the calculated rupture strain of the embedded reinforcement, and $\varepsilon_{rupt,bar}$ is the rupture strain of the bare reinforcement, both in millistrain; and $\gamma$ is the ratio between rupture strain of the embedded reinforcement and the rupture strain of the bare bar, $\varepsilon_{rupt,embed}/\varepsilon_{rupt,bar}$, assumed to be limited to between 0.33 and 1.0. The lower limit of 0.33 was chosen based on the regression line of fit, and the upper limit of 1.0 was chosen because the embedded rupture strain is assumed to not exceed the bare bar reinforcement rupture strain. This simplified reinforcement rupture formulation was then combined with the Bentz tension-stiffening model as an additional step to predicting reinforcement rupture for both smeared and discrete reinforcements.

To verify the proposed reinforcement rupture model, the seven uniaxial tension members used in the regression analysis were modeled. All FE analysis results using the proposed model matched experimental results reasonably well. Figure 2 gives a summary comparison between experimental member rupture strain and VecTor2-calculated rupture strain using both the Lee model and the proposed formulation; refer to Table E.1 in Appendix E. For this data set, the Lee model underestimates the rupture strain with a mean of 0.72, while the proposed formulation has a mean of 1.00. The Lee model also has a larger coefficient of variation (CoV) compared with the proposed formulation (17% compared with 13%).

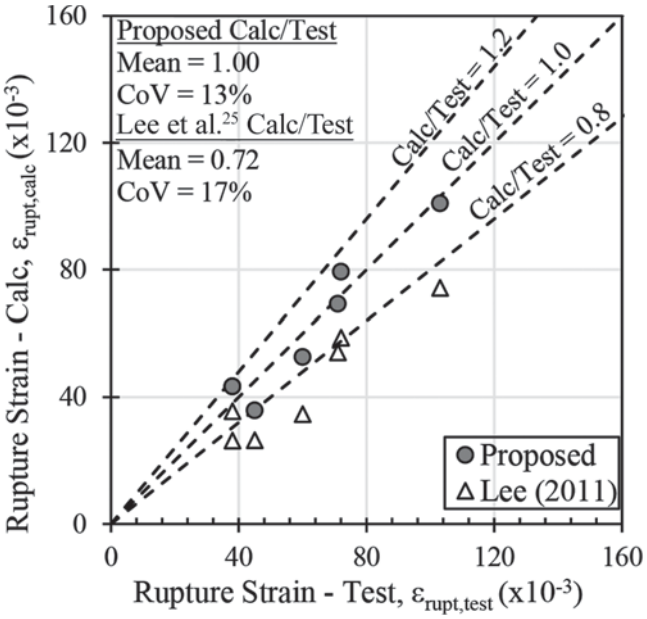


*Fig. 2—Embedded reinforcement rupture strains.*

### Average and maximum crack widths

When loaded under uniaxial tension, SFRC typically displays a strain-softening behavior, where the response is controlled by the localization of a single dominant crack. After cracking, the specimen's residual tensile stress never reaches the tensile strength and instead gradually reduces to zero. Because structural members will typically fail at the location of the largest crack, a maximum crack width calculation is presumed necessary to determine the resistance of a section. In conventional reinforced concrete, a characteristic crack width exists as $w_k$, which describes the crack width that only 5% of the cracks will exceed. The CEB-FIP estimates this characteristic crack width as 1.7 times the average crack width.[31] Deluce et al.[23] concluded, however, that due to crack localization, the ratio of maximum crack width to average crack width ($w_{cr,max}/w_{cr}$) for fiber-reinforced concrete is larger than that of conventional reinforced concrete. In addition, for a given strain, the fiber volume fraction, $V_f$, and the fiber aspect ratio, $l_f/d_f$, also influenced the maximum crack width; as fiber volume fraction or aspect ratio increases, the ratio of maximum to average crack width also increases. Thus, as per Deluce et al., the maximum crack width, $w_{cr,max}$ (mm), for fibrous concrete is calculated in VecTor2 as

$$w_{cr,max} = \left(1.7 + 3.4\frac{V_f l_f}{d_f}\right) w_{cr} \tag{18}$$

However, UHPFRC and some SFRC with high fiber content typically display strain-hardening behavior under uniaxial tension. In contrast to strain-softening materials, where crack localization occurs immediately after cracking, the tensile stress in strain-hardening materials continues to increase after cracking through the formation of multiple closely spaced narrow cracks.[32] The softening behavior associated with crack localization and fiber pullout occurs only after significant tensile straining. Because there is less tendency for cracks to localize in strain-hardening materials, the maximum crack limit introduced by Deluce et al. may unnecessarily limit the tensile stress attained by the fibers, and consequently, limit the tensile stress of the member. Thus, for strain-hardening materials such as UHPFRC, it is proposed that the maximum crack width reverts to 1.7 times the average crack width ($w_{cr,max} = 1.7w_{cr}$) until further research can provide a more definitive model. Thus, VecTor2 was modified such that the maximum crack width for fiber-reinforced concrete is calculated as

$$w_{cr,max} = \begin{cases} 1.7w_{cr} & \text{for strain-hardening material} \\ \left(1.7 + 3.4\dfrac{V_f l_f}{d_f}\right) w_{cr} & \text{for strain-softening material} \end{cases} \tag{19}$$

### Aggregate modeling

In conventional reinforced concrete, it is commonly observed that concrete mixtures containing coarser aggregates have higher shear resistance due to increases in aggregate interlock. However, due to the differences in thermal and mechanical properties between aggregates and cement paste, shear and tensile stresses may develop and result in microcracking at the interface zone. In the initial development of ultra-high-performance concrete, Richard and Cheyrezy[1] found that using fine quartz sand instead of coarse aggregates significantly reduced microcracking from external loads and autogenous shrinkage. Decreasing the aggregate size also enhanced the homogeneity in the cementitious matrix and produced better workability. In addition, smaller aggregate sizes caused less-frequent disturbances to the bond between fibers and the concrete matrix, improving the effective fiber bridging effect. As such, the coarsest aggregate size used in current UHPFRC mixtures generally lies between 0.5 and 4 mm (0.02 and 0.16 in.), with most being fine sand with a maximum diameter of less than 1 mm (0.04 in.).

As seen in the parametric study, the calculated shear behavior of UHPFRC is highly influenced by the assumed maximum aggregate size. The current models do not adequately consider the enhanced mechanical behavior of UHPFRC due to smaller aggregate sizes, such as the improved fiber bridging effect. In addition, the presence of fibers also provides the crack surface with sufficient roughness to compensate for the reduction in aggregate size. Accordingly, a preliminary model for effective aggregate size dependent on fiber properties was implemented. The proposed effective aggregate size, $a_{g,eff}$ (mm), as a function of $V_f$ and $l_f$, is formulated as follows

$$a_{g,eff} = \sum_{i=1}^{n} \frac{V_{f,i}}{0.02}\frac{l_{f,i}}{2} \tag{20}$$

where $V_{f,i}$ and $l_{f,I}$ are the volume fraction and length in mm of the $i$-th fiber reinforcement, respectively. Total $V_f$ is limited to 0.02.

To prevent this proposed aggregate size formulation from overestimating the improved effects of fibers on UHPFRC mechanical behavior, there also exists a maximum limit on the effective aggregate size, $a_{g,eff,max}$ (mm), taken as the minimum of half the fiber length or 10 mm (0.4 in.)

$$a_{g,eff} \le a_{g,eff,max} = \min\left(\frac{l_f}{2}, 10\text{ mm}\right) \quad (21)$$

The aggregate size, $a$ (mm), to be used in the MCFT and DSFM, is then taken as the maximum of the effective aggregate size calculated from Eq. (20) and (21) and the user-specified maximum aggregate size

$$a = \max\left(a_{g,eff}, input\right) \quad (22)$$

In the MCFT and DSFM, the aggregate size affects the constitutive relationships and the overall predicted behavior of a member through its influence on a variety of different mechanisms, such as in computing the crack spacing and crack width, maximum local shear stress at the crack, as well as fracture energy and the tension-softening response. However, fiber bond stresses, as shown in Appendix C, are calculated using the actual maximum aggregate size.

## VERIFICATION STUDIES

The efficacy of the revised constitutive models implemented in VecTor2 is first examined using the UHPFRC pure shear panels tested by Yap,[9] then further studied with experimental data from UHPFRC beam tests found in the literature.

VecTor2 contains a comprehensive selection of analysis models for various behavior mechanisms, with default selections available for each.[33] All the analysis models selected for the analyses reported herein were the default models except for the compression pre-peak and FRC tension responses. The Hoshikuma model, an exponential function, was taken as the ascending branch of the compression pre-peak response as this model is known to respond well to concrete with high compressive strengths. Both the VEM and the SDEM were considered in the verification study to account for the contribution of steel fiber reinforcement to concrete post-cracking tensile response. All material properties not provided by the experimental program were also assumed to be the VecTor2 default values.

In addition to the large-scale panel element tests, Yap[9] conducted flexural bending tests on prisms and uniaxial direct tension tests on dog-bone specimens for each panel using the same batch of UHPFRC. These were also modeled using SDEM and VEM. Model details and analysis results are provided in Appendix G.

### Modeling of shear panels

The UHPFRC shear panels tested by Yap[9] were modeled as a single four-node plane stress rectangular element with a dimension of 1000 x 1000 mm (39.4 x 39.4 in.) with thicknesses matching each panel's as-built thickness. The conventional and fiber reinforcement were modeled as smeared reinforcement embedded in the concrete. The lower-left corner of the element was restrained in both the x- and y-directions, while the lower-right corner was restrained in the y-direction only. The FE models were load-controlled with loads applied at the four nodes to create pure shear loading conditions. Monotonically increasing stress was applied, in 0.05 MPa (7.25 psi) increments, until failure.

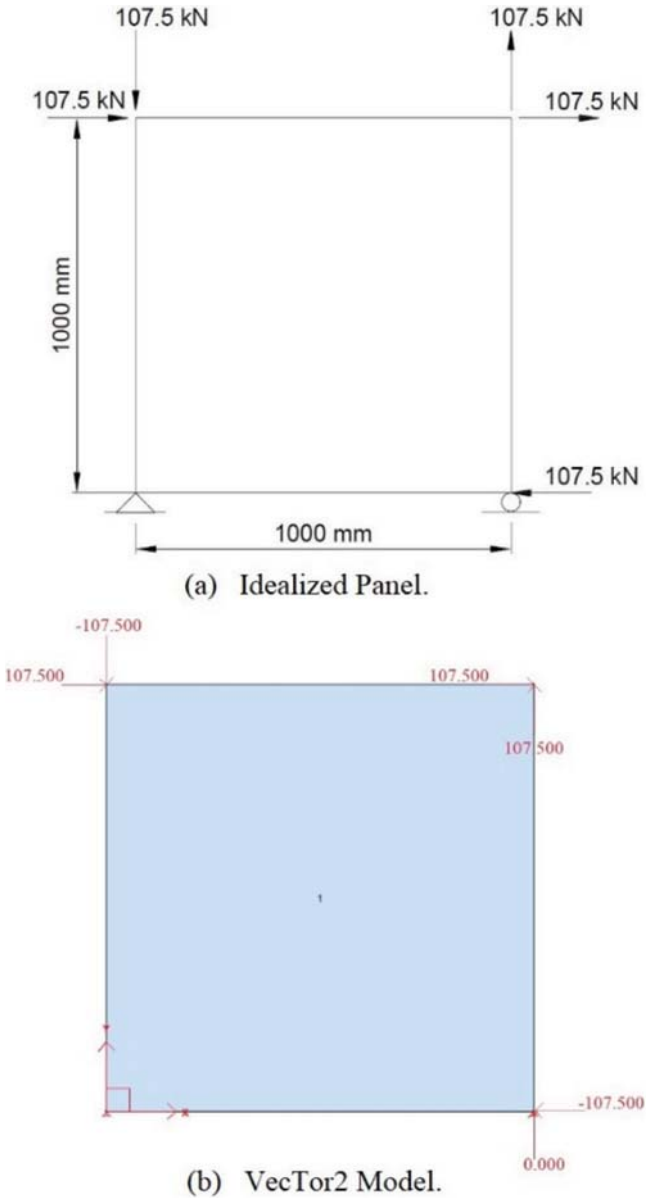


*Fig. 3—Single element model for Panel YS1.*

Figure 3 shows an example of the support and loading condition used for Panel YS1, which had a thickness of 215 mm (8.5 in.). (Recall from the parametric study that using a 10 x 10 element mesh produced identical results.)

All material properties available from the testing program were used in the FE models; refer to Appendix F. The input material parameters for the concrete and smeared reinforcement are given in Tables F.1 and F.2, respectively. The steel fiber properties are given in Table F.3. The maximum crack spacing in both the x- and y-directions was taken as the experimental value of 50 mm (2.0 in.).

Three series of analyses were conducted using, alternatively, the VEM, the SDEM, and custom input models for the tensile behavior of UHPFRC. The custom models were defined by data from the inverse analysis of prisms or from direct tension tests performed on material samples corresponding to the panel specimens; refer to Appendix G. That is, the peak stress-crack value, along with two other points taken from the post-peak stress-crack width tensile

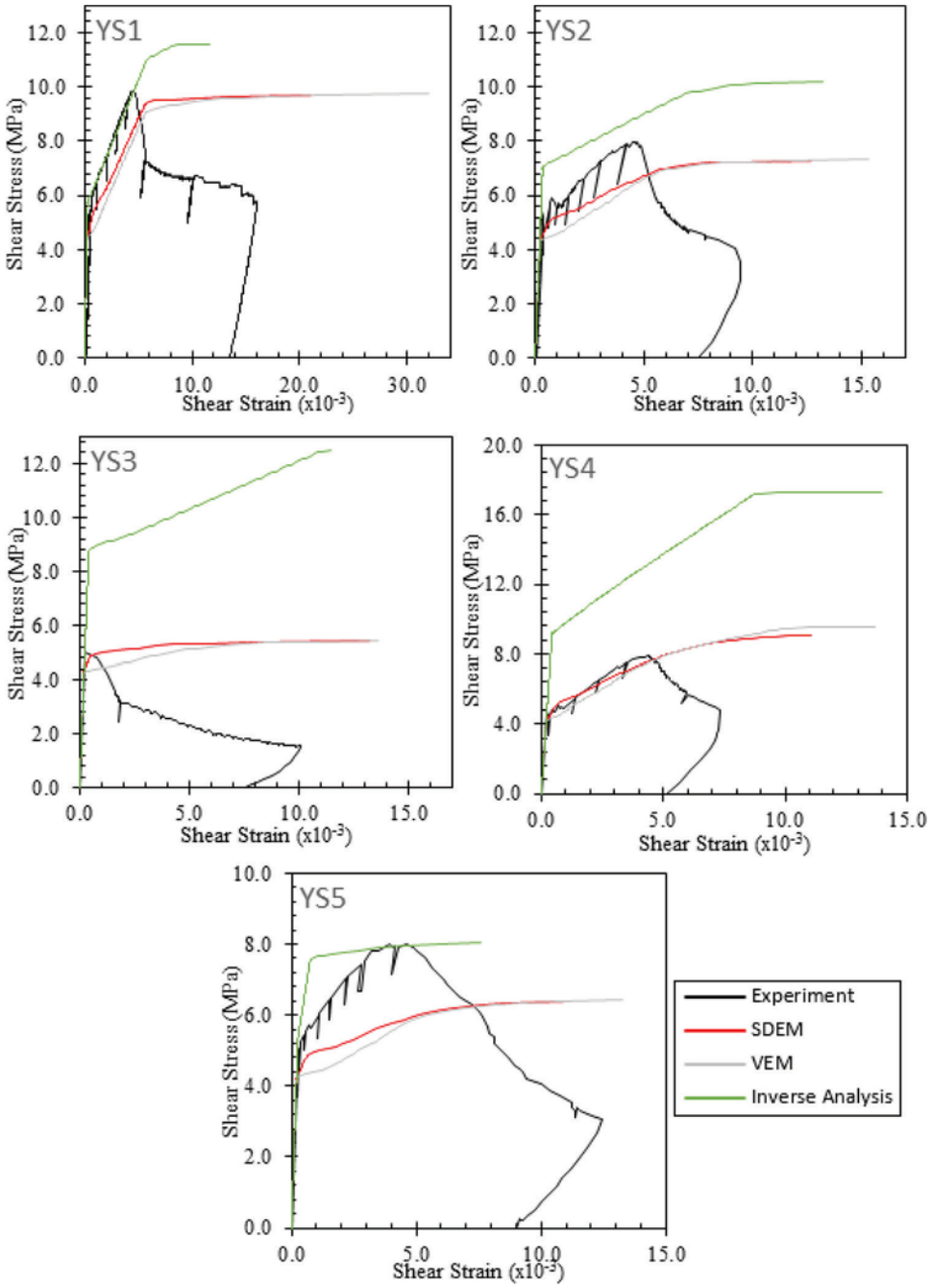


*Fig. 4—Experimental and VecTor2 response of UHPFRC pure shear panels.*

response in Fig. G.1 were manually entered into the tension-softening curve in VecTor2. The default VecTor2 cracking strength of $f_t' = 0.33\sqrt{f_c'}$ (MPa) previously used in each model was also replaced by the cracking stress determined from the inverse analysis of prism tests.

The modeling results obtained from the SDEM, VEM, and custom tension curves are compared with experimental results in Fig. 4. In general, the SDEM post-cracking pre-peak responses best aligned with the experimental results. Both the SDEM and VEM captured the initial pre-cracking shear stiffness well. The calculated cracking stress for SDEM and VEM was approximately 4.2 MPa (0.61 ksi) for the five panels, all lower than the reported experimental cracking stress. This was expected because these models used the default cracking strength available in VecTor2, which is commonly used for conventional reinforced concrete rather than UHPFRC. Similar to the SDEM and VEM results, the models using the inverse analysis and direct tension tests captured the pre-cracking shear stiffness well. However, the cracking stress estimated by the models that used inverse analysis ranged from 5.66 to 8.96 MPa (0.82 to 1.30 ksi), significantly higher than the reported panel experimental cracking stress. The custom tension model for panel YS5, which used the direct tension test properties, produced the most accurate estimate of cracking stress.

All FE models captured the post-cracking stiffness for all panels, except for YS3 and YS5. In Panel YS3, it was speculated that because this specimen did not contain any conventional reinforcement, there may have been a weak plane with fewer fibers, resulting in a strain-softening response after

**Table 1—Experimental simulated peak shear stress**

| | $\upsilon_{xy,u,exp}$ Experiment, MPa | $\upsilon_{xy,u,SDEM}$ SDEM, MPa | $\upsilon_{xy,u,VEM}$ VEM, MPa | $\upsilon_{xy,u,inv}$ Inverse, MPa | $\frac{\upsilon_{xy,u,SDEM}}{\upsilon_{xy,u,\exp}}$ | $\frac{\upsilon_{xy,u,VEM}}{\upsilon_{xy,u,exp}}$ | $\frac{\upsilon_{xy,u,inv}}{\upsilon_{xy,u,exp}}$ |
|---|---|---|---|---|---|---|---|
| Panel | (1) | (2) | (3) | (4) | (2)/(1) | (3)/(1) | (4)/(1) |
| YS1 | 9.90 | 9.68 | 9.73 | 11.59 | 0.98 | 0.98 | 1.17 |
| YS2 | 8.03 | 7.28 | 7.35 | 10.17 | 0.91 | 0.92 | 1.27 |
| YS3 | 4.99 | 5.41 | 5.44 | 12.5 | 1.08 | 1.09 | 2.51 |
| YS4 | 7.91 | 9.09 | 9.55 | 17.24 | 1.15 | 1.21 | 2.18 |
| YS5 | 8.04 | 6.38 | 6.47 | 8.03 | 0.79 | 0.80 | 1.00* |
| | | | | Mean | 0.98 | 1.00 | 1.62 |
| | | | | CoV | 14% | 16% | 41% |

Note: 1 MPa = 145 psi.

*Tensile properties from direct tension tests.

cracking. All models, however, showed strain-hardening responses. Although Panel YS5 showed a strain-hardening response similar to the other panels, the SDEM and VEM significantly underestimated their post-cracking stiffness, while the inverse analysis results overestimated the post-cracking stiffness. All models overestimated the panels' deformation capacity.

A comparison of the experimental and VecTor2 peak shear stresses, $v_{xy,u}$, is provided in Table 1. The average VecTor2 calculated-to-experimental ultimate capacity ratios for SDEM and VEM were 0.98 and 1.00, respectively. In contrast, the average calculated-to-experimental ultimate capacity using the custom tension curves extracted from the inverse analyses of test prism data was 1.62, a gross overestimation of capacity; in addition, the CoV of 41% suggests a weak correlation of results. Because the direct tension test results for Panel YS5 provided satisfactory results, the large deviations from experimental results when modeling with inverse analysis may be due to intrinsic flaws with the flexural prism testing and post-analysis procedure.

Overall, the models using inverse analysis results as input parameters in the tension-softening curve provided much poorer response calculations when compared to SDEM and VEM. The use of flexural prism test results in FE models produced a gross overestimation of UHPFRC behavior and is therefore not recommended for use in modeling in its current form. On the other hand, direct tension test results may aid in increasing the accuracy of FE models; further investigations are recommended.

## UHPFRC beams under flexure and shear

The enhancements to the constitutive models were also examined by comparing simulation results to the experimental results of 22 beam tests in previously published research programs. The details of the test specimens used are summarized in Appendix H (Table H.1). All beams were modeled in VecTor2 with specific dimensions according to each test specimen. The FE mesh consisted of four-node plane stress rectangular elements and three-node constant strain triangular elements, both with uniform thickness; typical meshes are shown in Fig. H.1. Two-node truss elements were used to model the longitudinal reinforcement. As bond failure was not observed in any test specimens, a perfect bond was assumed between the longitudinal reinforcing bar and the concrete. Fibers and shear reinforcement were modeled as smeared reinforcement within the concrete. Material properties were input as reported in the literature, including the concrete tensile strengths typically taken as determined from the inverse analyses of prism tests. Loading and support boundaries were modeled to represent actual experimental conditions, with the load in the FE models applied as a vertical displacement and increased monotonically until failure.

Figure 5 shows a comparison between the experimental and calculated ultimate capacities for all investigated UHPFRC beams. The analysis results suggest that both SDEM and VEM require additional improvements to accurately predict the behavior of largely flexure-critical UHPFRC specimens. Both models gave comparable results with a mean of 0.83 for the SDEM and 0.84 for the VEM. However, the VEM showed a slightly lower CoV of 22% than the SDEM CoV of 26%. It should be noted that all beams examined here had cross section depths of 270 mm (10.6 in.) or less, and that size effects may have contributed to the stronger than calculated strengths.

One potential reason for underestimating both the strength and ductility of flexure-critical UHPFRC beams is that the strain-hardening behavior may be limited due to the high input cracking strength and low fiber bond strength. To investigate this further, the modified material parameters proposed by Franssen et al.[19] in modeling UHPFRC-strengthened members were investigated for their applicability in modeling UHPFRC beams. Specifically, the bond strength increase to $\tau_{f,max} = 0.75\sqrt{f_c'}$ (MPa), and the simplified crack formulation of $s_{cr} = 0.75l_f$ were both adopted in this investigation. In addition, the concrete cracking strength input for all UHPFRC beams was reverted to the default cracking stress of $f_t' = 0.33\sqrt{f_c'}$ (MPa) to further ensure a strain-hardening response after cracking. The UHPFRC beams were then reanalyzed with these adjusted material inputs using the SDEM. The results show that overall, the modifications to the fiber bond strength and crack spacing significantly improved the post-cracking response of the UHPFRC beams. The average calculated-to-experimental

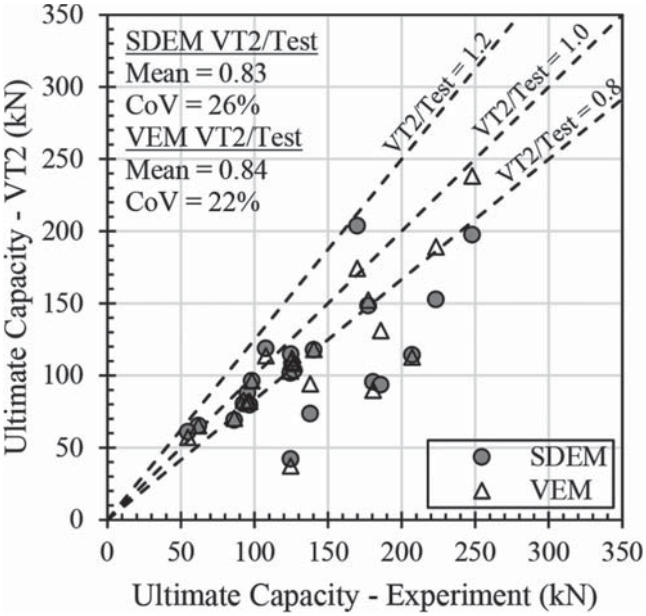


*Fig. 5—VecTor2-predicted ultimate capacity for UHPFRC beams.*

ultimate capacity ratio improved to 0.97, substantially better than the ratios previously produced by the SDEM and VEM of 0.83 and 0.84, respectively. The SDEM/Franssen results also showed a lower coefficient of variation of 22% compared with the SDEM CoV of 26%. This suggests that both higher bond stresses and lower crack spacing values may be warranted for UHPFRC; further investigations are required.

Finally, it should also be noted that the FE models were unable to accurately model the behavior of UHPFRC pure shear Panel YS3,[9] and UHPFRC Beams NR-1,2[11] and UH-N,[12] all of which had no conventional reinforcement. As such, recommendations for future work include further investigations on the effect of conventional reinforcement on modeled behavior.

## SUMMARY AND CONCLUSIONS

As a material, steel fiber-reinforced concrete (SFRC) is complex in its behavior and defies most current modeling efforts, as the results of the *fib* blind prediction competition clearly showed. Ultra-high-performance fiber-reinforced concrete (UHPFRC) is even less understood and merits additional experimental and numerical investigation. This study's main objective was to investigate, modify, and improve existing finite element (FE) analysis models in their capacity to represent shear-critical UHPFRC elements. Modifications were developed and implemented in nonlinear finite element analysis (NLFEA) program VecTor2. From the results of the analytical work performed, the following conclusions can be made:

1. The calculated post-cracking shear response of UHPFRC is significantly affected by maximum aggregate size, crack spacing and crack widths, and stochastic variations in material strengths. Thickness of the element, relative to fiber length, has a slighter influence. On the other hand, concrete tensile strength has little influence on the post-cracking response.

2. The Simplified Diverse Embedment Model (SDEM) and the Variable Engagement Model (VEM), two alternative constitutive models for SFRC, can be extended to capture the response of UHPFRC pure shear panels sufficiently well. This improvement is accomplished by including an effective aggregate size calculation and modifying the maximum crack width formulation for UHPFRC.

3. The reinforcement rupture formulation developed from regression analysis improves the prediction of rupture strain in reinforced concrete specimens experiencing tension.

4. Using post-cracking tension models derived from the inverse analysis of test prisms can lead to grossly unconservative predictions of strength and ductility. In contrast, using the results from direct tension test specimens in a custom tension curve may increase the accuracy of the FE models.

5. Despite the modifications made through this study, the SDEM and VEM, as currently configured and calibrated, still lack sufficient accuracy when applied to UHPFRC. Although the simulation results for large-scale shear-critical UHPFRC panels were strong, the strengths and post-cracking stiffnesses calculated for small-scale flexure-critical UHPFRC beams were less satisfactory.

6. As per Franssen et al.,[19] increasing the fiber bond stress and modifying the crack spacing parameter can lead to substantially improved results. Thus, the SDEM and VEM may be potentially viable platforms for accurately modeling UHPFRC beams provided that better models for fiber bond stress and crack spacing are developed.

These conclusions were derived from studies based on sparse test data. Additional experimental and analytical research is required.

## AUTHOR BIOS

**Zhongyue Zhang** *is a Junior Bridge Engineer at AECOM in Edmonton, AB, Canada. She received her BSc in civil engineering from the University of Alberta, Edmonton, AB, Canada, and her MASc in civil engineering from the University of Toronto, Toronto, ON, Canada. Her research interests include shear behavior of reinforced concrete and nonlinear finite element modeling of fiber-reinforced concrete.*

**Frank J. Vecchio**, *FACI, is a Professor in the Department of Civil Engineering at the University of Toronto. He is a past member of Joint ACI-ASCE Committees 441, Reinforced Concrete Columns, and 447, Finite Element Analysis of Reinforced Concrete Structures. He is a recipient of the ACI Structural Research (1998), Structural Engineering (1999), Wason Medal (2011), Joe Kelley (2016), and Arthur J. Boase (2020) awards. His research interests include advanced constitutive modeling and analysis of reinforced concrete and assessment and rehabilitation of structures.*

**Evan C. Bentz**, *FACI, is Professor and Associate Chair of Civil Engineering at the University of Toronto. He received his BASc from the University of Waterloo, Waterloo, ON, Canada, in 1994, and his PhD from the University of Toronto in 2000. He is a member of ACI Committee 445, Shear and Torsion and is a member and former chair of ACI Committee 365, Service Life Modelling. He received the ACI Chester Paul Seiss Award in 2018 and the ACI Design Award twice.*

*ACI member* **Stephen J. Foster** *is Acting Dean of Engineering at the University of New South Wales (UNSW) Sydney, NSW, Australia, and is the elected Deputy President of the International Federation for Structural Concrete (*fib*). His research interests include bringing new material technologies to the design of concrete structures, including fiber and ultra-high-performance concrete, geopolymer and alkaline activated concretes, and high-strength concretes and reinforcing steels.*

## ACKNOWLEDGMENTS

This project was funded by the Australian Research Council (ARC) Discovery Grant DP170104618; the support of the ARC is gratefully acknowledged.

## REFERENCES

1. Richard, P., and Cheyrezy, M., "Composition of Reactive Powder Concretes," *Cement and Concrete Research*, V. 25, No. 7, 1995, pp. 1501-1511. doi: 10.1016/0008-8846(95)00144-2

2. Roux, N.; Andrade, C.; and Sanjuan, M. A., "Experimental Study of Durability of Reactive Powder Concretes," *Journal of Materials in Civil Engineering*, ASCE, V. 8, No. 1, 1996, pp. 1-6. doi: 10.1061/(ASCE)0899-1561(1996)8:1(1)

3. Bonneau, O.; Lachemi, M.; Dallaire, E.; Dugat, J.; and Aïtchin, P. C., "Mechanical Properties and Durability of Two Industrial Reactive Powder Concretes," *ACI Materials Journal*, V. 94, No. 4, July-Aug. 1997, pp. 286-290.

4. Voo, Y. L., and Foster, S. J., "Characteristics of Ultra-High Performance 'Ductile' Concrete and Its Impact on Sustainable Construction," *The IES Journal Part A: Civil & Structural Engineering*, V. 3, No. 3, 2010, pp. 168-187. doi: 10.1080/19373260.2010.492588

5. Barros, J.; Sanz, B.; Kabele, P.; Yu, R.; Meschke, G.; Planas, J.; Cunha, V.; Caggiano, A.; Ozyurt, N.; Ventura-Gouveia, A.; van den Bos, A.; Poveda, E.; Gal, E.; Cervenka, J.; Neu, G.; Rossi, P.; Dias-da-Costa, D.; Juhasz, P.; Cendon, D.; Ruiz, G.; and Valente, T., "Blind Competition on the Numerical Simulation of Steel-Fiber-Reinforced Concrete Beams Failing in Shear," *Structural Concrete*, V. 22, No. 2, 2020, pp. 939-967. doi: 10.1002/suco.202000345

6. Vecchio, F. J., "VecTor2 Nonlinear Finite Element Analysis," 2000.

7. Vecchio, F. J., and Collins, M. P., "Modified Compression Field Theory for Reinforced Concrete Elements Subjected to Shear," *ACI Journal Proceedings*, V. 83, No. 2, Mar.-Apr. 1986, pp. 219-231.

8. Vecchio, F. J., "Disturbed Stress Field Model for Reinforced Concrete: Formulation," *Journal of Structural Engineering*, ASCE, V. 126, No. 9, 2000, pp. 1070-1077. doi: 10.1061/(ASCE)0733-9445(2000)126:9(1070)

9. Yap, B., "Behaviour of Ultra High Performance Fibre Reinforced Concrete Subjected to Pure Shear," master's thesis, University of Toronto, ON, Canada, 2020, 169 pp.

10. Yoo, D. Y., and Yoon, Y. S., "Structural Performance of Ultra-High-Performance Concrete Beams with Different Steel Fibers," *Engineering Structures*, V. 102, Nov. 2015, pp. 409-423. doi: 10.1016/j.engstruct.2015.08.029

11. Yang, I. H.; Joh, C.; and Kim, B. S., "Structural Behavior of Ultra High Performance Concrete Beams Subjected to Bending," *Engineering Structures*, V. 32, No. 11, 2010, pp. 3478-3487. doi: 10.1016/j.engstruct.2010.07.017

12. Yoo, D. Y.; Banthia, N.; and Yoon, Y. S., "Experimental and Numerical Study on Flexural Behavior of Ultra-High-Performance Fiber-Reinforced Concrete Beams with Low Reinforcement Ratios," *Canadian Journal of Civil Engineering*, V. 44, No. 1, 2016, pp. 18-28. doi: 10.1139/cjce-2015-0384

13. Singh, M.; Sheikh, A. H.; Mohamed Ali, M. S.; Visintin, P.; and Griffith, M. C., "Experimental and Numerical Study of the Flexural Behaviour of Ultra-High Performance Fibre Reinforced Concrete Beams," *Construction and Building Materials*, V. 138, May 2017, pp. 12-25. doi: 10.1016/j.conbuildmat.2017.02.002

14. Kodur, V.; Solhmirzaei, R.; Agrawal, A.; Aziz, E. M.; and Soroushian, P., "Analysis of Flexural and Shear Resistance of Ultra High Performance Fiber Reinforced Concrete Beams without Stirrups," *Engineering Structures*, V. 174, Nov. 2018, pp. 873-884. doi: 10.1016/j.engstruct.2018.08.010

15. Foster, S. J.; Voo, Y. L.; and Chong, K. T., "FE Analysis of Steel Fiber Reinforced Concrete Beams Failing in Shear: Variable Engagement Model," *Finite Element Analysis of Reinforced Concrete Structures*, SP-237, L. Lowes and F. Filippou, eds., American Concrete Institite, Farmington Hills, MI, 2006, pp. 55-70.

16. Voo, Y. L.; Poon, W. K.; and Foster, S. J., "Shear Strength of Steel Fiber-Reinforced Ultrahigh-Performance Concrete Beams without Stirrups," *Journal of Structural Engineering*, ASCE, V. 136, No. 11, 2010, pp. 1393-1400. doi: 10.1061/(ASCE)ST.1943-541X.0000234

17. Voo, Y. L.; Foster, S. J.; and Gilbert, R. I., "Shear Strength of Fiber Reinforced Reactive Powder Concrete Prestressed Girders without Stirrups," *Journal of Advanced Concrete Technology*, V. 4, No. 1, 2006, pp. 123-132. doi: 10.3151/jact.4.123

18. Chen, L., and Graybeal, B. A., "Modeling Structural Performance of Ultrahigh Performance Concrete I-Girders," *Journal of Bridge Engineering*, ASCE, V. 17, No. 5, 2011, pp. 754-764. doi: 10.1061/(ASCE)BE.1943-5592.0000305

19. Franssen, R.; Guner, S.; Courard, L.; and Mihaylov, B., "A Study on the Numerical Modelling of UHPFRC-Strengthened Members (ICCRRR 2018)," *MATEC Web of Conferences*, V. 199, No. 09001, 2018, pp. 1-10.

20. Voo, J. Y. L., and Foster, S., "Variable Engagement Model for the Design of Fibre Reinforced Concrete Structures," *Proceedings*, Advanced Materials for Construction of Bridges, Buildings, and Other Structures III, Davos, Switzerland, 2003, pp. 1-11.

21. Lee, S. C.; Cho, J. Y.; and Vecchio, F. J., "Diverse Embedment Model for Steel Fiber-Reinforced Concrete in Tension: Model Verification," *ACI Materials Journal*, V. 108, Sept-Oct. 2011, pp. 526-535.

22. Lee, S. C.; Cho, J. Y.; and Vecchio, F. J., "Simplified Diverse Embedment Model for Steel Fiber-Reinforced Concrete Elements in Tension," *ACI Materials Journal*, V. 110, No. 4, July-Aug. 2013, pp. 403-412.

23. Deluce, J. R.; Lee, S. C.; and Vecchio, F. J., "Crack Model for Steel Fiber-Reinforced Concrete Members Containing Conventional Reinforcement," *ACI Structural Journal*, V. 111, No. 1, Jan.-Feb. 2014, pp. 93-102.

24. Hunter, M. D., "Towards Stochastic Finite Element Analysis of Reinforced Concrete Structures," master's thesis, University of Toronto, Toronto, ON, Canada, 2016, 262 pp.

25. Lee, S. C.; Cho, J. Y.; and Vecchio, F. J., "Model for Post-Yield Tension Stiffening and Rebar Rupture in Concrete Members," *Engineering Structures*, V. 33, No. 5, 2011, pp. 1723-1733. doi: 10.1016/j.engstruct.2011.02.009

26. Bentz, E. C., "Explaining the Riddle of Tension Stiffening Models for Shear Panel Experiments," *Journal of Structural Engineering*, ASCE, V. 131, No. 9, 2005, pp. 946-955. doi: 10.1061/(ASCE)0733-9445(2005)131:9(1422)

27. Mayer, U., and Eligehausen, R., "Bond Behaviour of Ribbed Bars at Inelastic Steel Strains," *Proceedings of the Second International PhD Symposium in Civil Engineering*, Budapest, Hungary, 1998, pp. 1-8.

28. Moreno, D. M.; Trono, W.; Jen, G.; Ostertag, C.; and Billington, S. L., "Tension Stiffening in Reinforced High Performance Fiber Reinforced Cement-Based Composites," *Cement and Concrete Composites*, V. 50, July 2014, pp. 36-46. doi: 10.1016/j.cemconcomp.2014.03.004

29. Kang, S. B.; Tan, K. H.; Zhou, X. H.; and Yang, B., "Influence of Reinforcement Ratio on Tension Stiffening of Reinforced Engineered Cementitious Composites," *Engineering Structures*, V. 141, June 2017, pp. 251-262. doi: 10.1016/j.engstruct.2017.03.029

30. Nguyen, W.; Bandelt, M. J.; Trono, W.; Billington, S. L.; and Ostertag, C. P., "Mechanics and Failure Characteristics of Hybrid Fiber-Reinforced Concrete (HyFRC) Composites with Longitudinal Steel Reinforcement," *Engineering Structures*, V. 183, Mar. 2019, pp. 243-254. doi: 10.1016/j.engstruct.2018.12.087

31. Comite Euro-International Du Beton, "Model Code for Concrete Structures: CEB-FIP International Recommendations," CEB-FIP, Paris, France, 1978.

32. Naaman, A. E., "High Performance Fiber Reinforced Cement Composites: Classification and Applications," *Proceedings of the CBM-CI International Workshop*, Karachi, Pakistan, 2008, pp. 289-401.

33. Wong, P.; Vecchio, F.; and Trommels, H., "VecTor2 & Formworks User's Manual," 2nd Edition, University of Toronto, ON, Canada, 2013.